CrossMark

Additive Manufacturing of Three-Phase Syntactic Foams Containing Glass Microballoons and Air Pores

ASHISH KUMAR SINGH,[1,4] ALEXANDER J. DEPTULA,[2]
RAJESH ANAWAL,[3] MRITYUNJAY DODDAMANI,[3] and
NIKHIL GUPTA[1]

1.—Composite Materials and Mechanics Laboratory, Mechanical and Aerospace Engineering Department, New York University, Tandon School of Engineering, Brooklyn, NY 11201, USA. 2.—Rose-Hulman Institute of Technology, 5500 Wabash Ave, Terre Haute, IN 47803, USA 3.—Advanced Manufacturing Laboratory, Department of Mechanical Engineering, National Institute of Technology Karnataka, Surathkal, India. 4.—e-mail: aksingh@nyu.edu

High-density polyethylene and its syntactic foams reinforced with 20 vol.% and 40 vol.% glass microballoons were 3D printed using the fused filament fabrication method and studied for their compressive response. The three-phase microstructure of syntactic foams fabricated in this work also contained about 10 vol.% matrix porosity for obtaining light weight for buoyancy applications. Filaments for 3D printing were developed using a single screw filament extruder and printed on a commercial 3D printer using settings optimized in this work. Three-dimensional printed blanks were machined to obtain specimens that were tested at 10^{-4} s^{-1}, 10^{-3} s^{-1}, 10^{-2} s^{-1} and 1 s^{-1} strain rates. The compression results were compared with those of compression-molded (CM) specimens of the same materials. It was observed that the syntactic foam had a three-phase microstructure: matrix, microballoons and air voids. The air voids made the resulting foam lighter than the CM specimen. The moduli of the 3D-printed specimen were higher than those of the CM specimens at all strain rates. Yield strength was observed to be higher for CM samples than 3D-printed ones.

INTRODUCTION

Syntactic foams are a class of lightweight porous composite materials synthesized by dispersing hollow particles in a matrix material.[1] The shell of the hollow particles provides a reinforcing effect to each pore present in these composite foams.[2] The filler content, material and shell thickness are among the parameters that can be used to control the properties of syntactic foams over a wide range.[3–7] Thermoplastic matrix syntactic foams have been fabricated by methods such as extrusion,[8] injection molding [9] and compression molding.[10] Each of these methods leads to fracture of some particles during processing. In addition, lower density of hollow particles compared with the matrix resin may also lead to segregation if a low volume fraction of particles is used in these composites. Additive manufacturing (AM) methods provide advantages in many such scenarios, especially when syntactic foams of low hollow particle volume fractions are required or when complex-shaped components are to be manufactured.[11]

Recent studies have demonstrated the possibility of using additive manufacturing methods for composite materials such as carbon/glass-reinforced polymer composites[12–14] or syntactic foams.[15] The fused filament fabrication (FFF) method has been used for this purpose with a high-density polyethylene (HDPE) matrix and fly ash cenosphere reinforcement. The first step of such studies is to extrude a high-quality filament containing the desired volume fraction of hollow particles.[16] Optimization of extrusion parameters such as temperature and screw speed provided a high-quality filament, which could be used for three-dimensional (3D) printing using a commercial FFF printer. Challenges related to adhesion of the first printed layer to the build plate, warpage of the syntactic foam piece during heating and cooling effects during

printing and dimensional tolerances are some of the key issues that need attention during the 3D printing process. Previous studies on HDPE matrix syntactic foams showed that the 3D-printed components have higher tensile properties in the printing direction compared with the injection and compression-molded syntactic foams of the same composition.[15] The improvement in the properties was attributed to two factors: (1) improved bonding at the particle–matrix interface and (2) alignment of polymer chains during the extrusion process of filament manufacturing and 3D printing.

Obtaining low density in syntactic foams is of great interest in weight-sensitive applications. Incorporation of hollow particles has a limit on density reduction. Further reduction in density requires innovative methods. In this context, three-phase syntactic foams have been studied, where a limited amount of air porosity is also embedded in the matrix material.[17,18] These three-phase foams are considered useful for underwater applications, potentially suitable for sub-4000-m range buoyancy modules. The present study is focused on developing a three-phase syntactic foam filament and studying the compressive properties of 3D-printed specimens. The emphasis of the study is to use a commercial FFF printer without any hardware modification for 3D printing of syntactic foam components. Since FFF is a high-temperature extrusion process, the porosity embedded in the filament may completely collapse and may not translate in the final part. Hence, process control is required not only in filament manufacture but also in the 3D printing process to preserve the three-phase syntactic foam microstructure in the printed component.

MATERIALS AND METHODS

Filament and 3D Printing

HDPE resin of grade HD50MA180 (20 g/10 min melt flow index and 97,500 g/mol mean molecular weight) was used as the matrix material. The resin was procured from Reliance Polymers, Mumbai, India. Glass microballoons (GMBs) of grade SID350 (nominal true particle density of 0.350 g/cm^3 and mean particle size of 45 μm) were provided by Trelleborg Offshore, USA. The syntactic foams consisted of 20 vol.% and 40 vol.% GMBs in HDPE matrix and are referred to as H350-20 and H350-40, respectively. These materials have been used in previous studies where syntactic foams were produced by injection and compression molding methods.[19,20] Those available results will help in comparing the properties of the present set of syntactic foams synthesized by 3D printing.

In the first step, GMB/HDPE blends were prepared using a Brabender (Plasticoder, Western Company Keltron CMEI, Germany, Model 16CME SPL). Measured quantities of HDPE and GMB were fed into the Brabender hopper. The blending temperature and screw speed of 160°C and 10 rpm, respectively, optimized from an initial set of experiments, were used for mixing to minimize the particle breakage.[10] The GMB/HDPE blend was then fed into a single screw extruder (Aasabi Machinery Pvt. Ltd., India, Model 25SS/MF/26). Average barrel and die temperatures were maintained at 160°C and 150°C, respectively, during filament extrusion. The screw speed was maintained at 20 rpm, and the corresponding take-off speed was set at 21.3 rpm to get a filament diameter of 1.75 ± 0.03 mm. The chosen screw speed and temperature parameters helped in retaining and entrapping the air porosity in the filament during the extrusion process.

Flashforge CreatorPro was used to print the samples with a 0.4-mm-diameter printing nozzle to avoid blockage due to the presence of GMB in the HDPE matrix. HDPE tape was applied to the build plate to ensure proper part adhesion during the 3D printing process. Cylinders with 15 mm diameter and 50 mm height were printed using HDPE, H350-20 and H350-40 and subsequently machined to produce compression specimens. A representative 3D-printed cylinder and machined compression specimen are shown in Figure S1 in the supplementary material. Parts were printed at 225°C for neat HDPE and 235°C for the syntactic foams. Layer height for the parts was 0.67 mm, and 100% infill was used to ensure that only the porosity that exists inside the filament is translated to the printed part and additional pores between the deposition layers are not created.

Quasi-Static Compression

Quasi-static compression tests were carried out on an Instron 4467 universal testing machine with a 30-kN load cell at three different strain rates of 10^{-4} s^{-1}, 10^{-3} s^{-1} and 10^{-2} s^{-1}. The data were acquired using Bluehill 2.0 software and analyzed using an in-house-developed MATLAB code. In addition, a dynamic load cell (PCB 208C03, 2.224 kN) was used with the Instron frame to test specimens at 1 s^{-1} strain rate, and data were collected using an oscilloscope. Quasi-static compression tests were performed on specimens of 8 mm diameter and 4 mm height. Smaller specimens with diameter and height of 4 mm were printed to test at 1 s^{-1} because of the lower load capacity of the dynamic load cell. Yield strength was computed using the 0.2% offset method. At least five specimens were tested for each material type and strain rate, and average and standard deviations for various compressive properties are reported.

Imaging

A Hitachi S3400-N scanning electron microscope (SEM) equipped with backscatter and secondary electron detectors was used to obtain micrographs of the material surfaces. The specimens were coated

with a layer of gold using a Cressington 108 Auto Sputter coater. All types of as-manufactured specimens were freeze fractured using liquid nitrogen for SEM imaging.

A Bruker Skyscan 1172 micro-CT with 10-W x-ray source and 4-K CCD x-ray camera was used to perform x-ray CT scanning. Specimens of 3D-printed foams with 2 mm diameter and 4 mm length were machined for CT scanning. This small size was chosen to obtain the highest possible resolution. The pixel size of the images obtained was 0.54 μm with 4 K resolution (4000 × 2664 pixels). The x-ray source was set at 21 kV and 110 μA, and the specimens were exposed for 1850 ms. The x-ray projections were then reconstructed using Bruker NRecon, and images were processes using ImageJ software.

RESULTS

Density and Microstructure

The expected microstructure of three-phase syntactic foams is schematically represented in Fig. 1a. Presence of matrix porosity can be determined by density measurements. The densities of the HDPE, H350-20 and H350-40 filaments were measured as 0.945 ± 0.052 g/cm^3, 0.808 ± 0.048 g/cm^3 and 0.708 ± 0.055 g/cm^3, respectively. Compared with the theoretical densities calculated on the basis of the resin and GMB volume fractions present in these specimens, the measured density values are 10.5%, 11.6% and 8.5% lower than the theoretical densities of the respective materials. This difference can be attributed to the porosity entrapped within the filament during the filament extrusion process. This calculation assumes that no GMB fracture has occurred during processing. However, in practice, some GMBs fracture, so this calculation underestimates the matrix porosity. A low-magnification SEM of the cross-section of a representative H350-20 filament is shown in Fig. 1b. The circular cross-section of the filament can be observed in this figure. A higher magnification image of the same filament in Fig. 1c shows dispersed GMBs and scattered air pores, providing evidence of the three-phase syntactic foam microstructure. A similar microstructure is also observed for H350-40 filament in Fig. 1d. Close observations of the microstructures reveal that the filament core seems to have greater matrix porosity compared with the outer rim, which is attributed to the flow of polymer material along the barrel of the extruder making a film on the filament that entraps the porosity inside. The extruder die has a converging conical zone leading to the nozzle exit. As material flows through this zone, the porosity is gradually pushed radially inwards leading to a greater concentration in the core. These filaments are used for 3D printing of syntactic foam specimens for compression testing.

The 3D-printed parts of HDPE, H350-20 and H350-40 have densities of 0.943 ± 0.009 g/cm^3, 0.776 ± 0.006 g/cm^3 and 0.710 ± 0.028 g/cm^3, respectively. The densities of the printed part are 10.7%, 15.2% and 8.2% lower for HDPE, H350-20 and H350-40 specimens than the respective values expected from the rule of mixtures. The density values of the printed parts are close to the respective values measured for the developed filaments, indicating that the matrix porosity survived the 3D printing process. The micrographs of freeze-fractured 3D-printed specimens of the H350-20 and H350-40 specimens are shown in Fig. 1e and f, respectively. The entrapped air pores can be observed in these images as well. Comparison of Fig. 1e and f reveals that the air pores are circular in H350-20, while the pores are elongated in the H350-40 specimen. This was confirmed by performing micro-CT scanning on the 3D-printed specimen. Figure 2 shows the comparison between the shape and size of the porosity within the two materials. H350-20 has more circular, larger and fewer pores, as opposed to H350-40, which has more, smaller and irregularly shaped pores. Due to irregular shape of the pores and very thin walls of GMBs, the porosity is not quantitatively calculated. The wall thickness of GMBs is below the resolution limit of the CT scan and cannot be reliably identified. It is likely that a higher volume fraction of GMB in H350-40 affects the rheology of the material and makes it difficult for it to flow. Such an effect would prevent the particles from reorganizing the material to make pores more circular. However, printing conditions such as printing temperature, printing speed, build plate temperature and cooling rate are expected to affect the size and shape of the air pores, and further optimization can be conducted on obtaining a specific size and shape as desired.

Compressive Response

The compressive stress–strain responses of 3D-printed HDPE and syntactic foams at different strain rates are presented in Fig. 3. All three materials show a clear trend in stress–strain response with respect to strain rate, where modulus and strength are found to increase with strain rate. A similar trend was observed in injection-molded HDPE and syntactic foams in previous studies.[21] Note that those previous studies were focused on fully dense HDPE and two-phase syntactic foams. One of the important characteristics of syntactic foams, and porous materials in general, is the stress plateau region under compressive loading conditions,[19,21] which leads to low strain hardening and high energy absorption capabilities in these materials through plastic deformation and porosity densification. As the GMB volume fraction increases, the plateau region become more prominent, which is also observed in the compressive behavior of 3D-printed syntactic foams. The compressive properties extracted from the stress–strain graphs are listed in Table I. It is observed that the elastic modulus
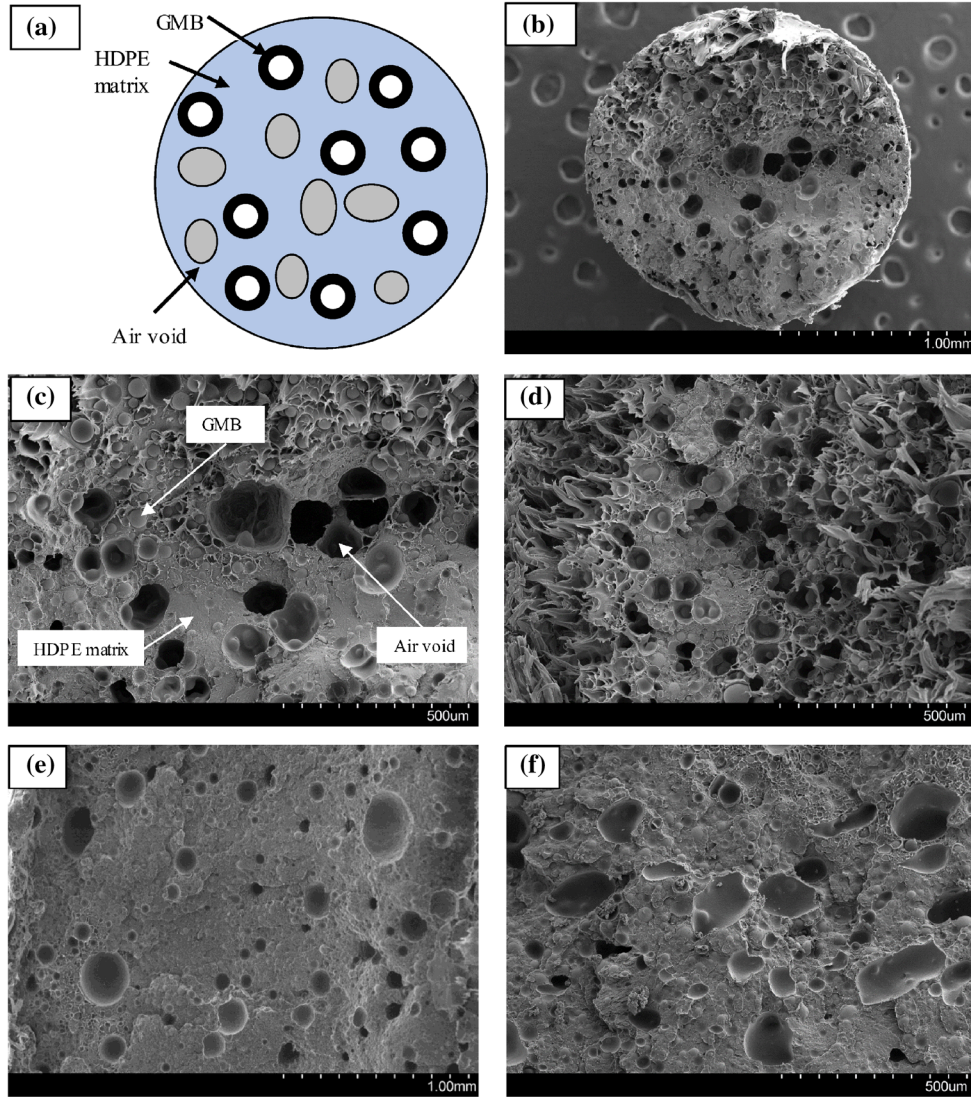
Fig. 1. Schematic representation of the three-phase microstructure of syntactic foam filaments. SEM micrographs of (b) the circular cross-section of H350-20 filament, three-phase microstructure of (c) H350-20 filament, (d) H350-40 filament, (e) 3D-printed H350-20 and (f) 3D-printed H350-40.

increases with strain rate for HDPE and syntactic foams because of the viscoelastic nature and low glass transition temperature of HDPE resin.[22] Although all the strain rates selected in the present work are within the quasi-static regime, the materials still show remarkable strain rate sensitivity, which has been of great interest for polymers in recent studies.[23–25] The yield strength of syntactic foams is comparable to HDPE resin at similar strain rates. This observation is important because syntactic foams have low density, and their use in underwater applications can provide weight-saving benefits, as can be envisioned from the specific yield strength column in Table I. It is also observed that the specific elastic modulus and strength for syntactic foams are higher compared with the HDPE resin, which can be beneficial in weight-sensitive applications and buoyancy modules.

SEM images of compression-tested 3D-printed H350-20 and H350-40 are shown in Fig. 4 for the 10^{-3} s^{-1} strain rate. These figures show the absence of matrix porosity due to compaction under compression. Since GMBs have high stiffness, the matrix pores are the first to collapse in the material, leading to initial densification. Once the matrix porosity has densified, the stress level increases, and the GMB crushing leads to further densification. Broken GMBs are also visible in the matrix. Extensive plastic deformation of the matrix resin is visible in low-magnification micrographs. Since all the compression tests are conducted within the quasi-static strain rate range, there is no remarkable difference in the appearance of the fracture surface for these materials with respect to strain rate. The stress–strain graphs show a similar level of strains in all the specimens at all strain rates by
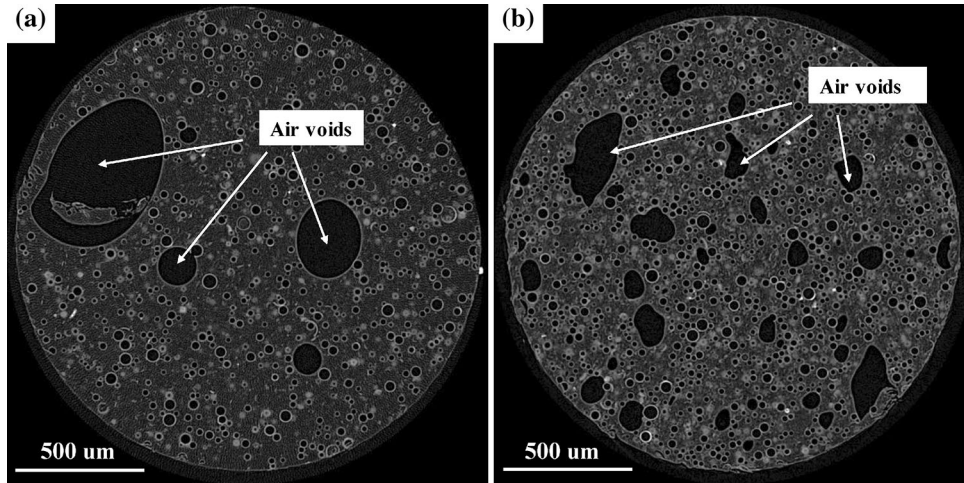
Fig. 2. Reconstructed micro-CT scan sliced images of 3D-printed (a) H350-20 and (b) H350-40 syntactic foams showing the matrix, hollow particles and air voids.
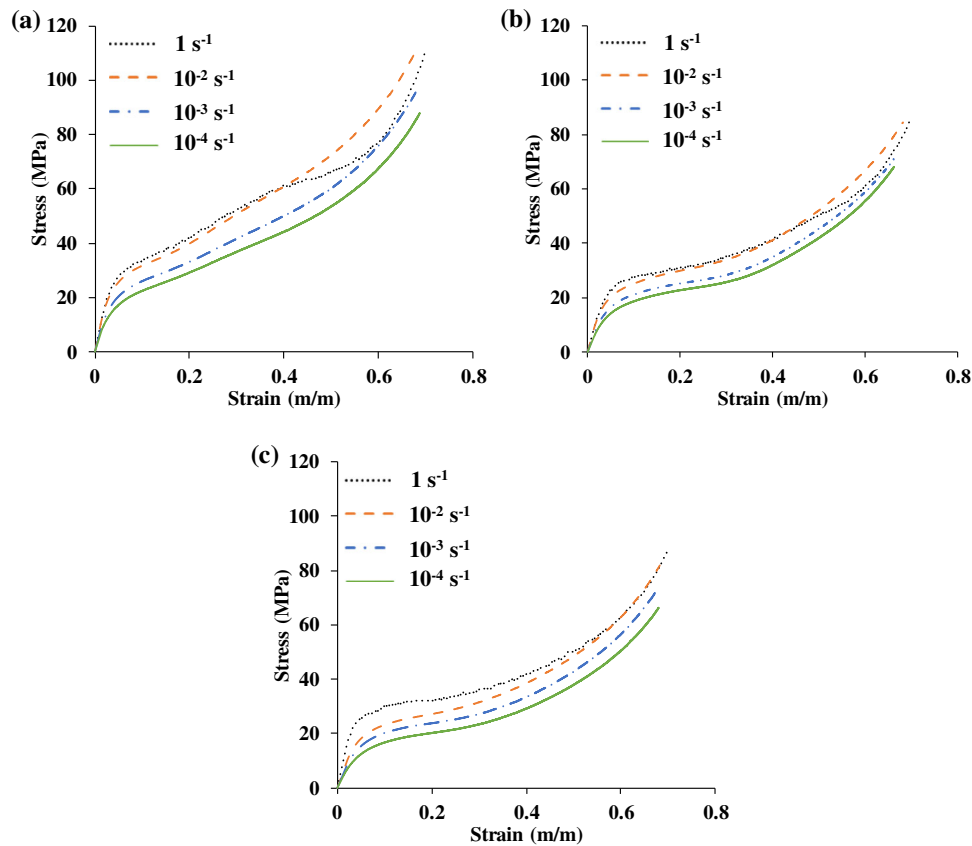

Fig. 3. Stress-strain curves at varying strain rates for (a) neat HDPE, (b) H350-20 and (c) H350-40.

the time the tests were discontinued. Therefore, the extent of plastic deformation and densification features are also similar.

DISCUSSION

The trends observed in mechanical properties in Table I are further analyzed in Fig. 5. The moduli of the materials follow an increasing trend with strain rate as shown in Fig. 5a. This strain rate sensitivity of the modulus in polymer matrix syntactic foams has been previously observed.[15,19] It can be seen that HDPE has the highest modulus followed by H350-20 and H350-40 at all strain rates. This trend is opposite to what was observed in compression-molded specimens,[19] where the syntactic foams showed a higher modulus than the neat HDPE. This trend is likely observed because of the presence

Table I. Mechanical properties measured from quasi-static compression testing of 3D-printed HDPE and its syntactic foams

Material	Strain rate (s^{-1})	Modulus (MPa)	Yield strength (MPa)	Specific modulus (MPa-cm^3/g)	Specific yield strength (MPa-cm^3/g)	Yield strain (%)	Energy absorbed till 50% strain (MJ/m^3)
HDPE	1	923 ± 36	15.5 ± 0.5	980 ± 38	16.5 ± 1.7	1.8 ± 0.1	23.7 ± 0.6
	10^{-2}	821 ± 69	12.2 ± 1.0	872 ± 73	13.0 ± 1.1	1.8 ± 0.1	22.3 ± 0.4
	10^{-3}	686 ± 31	11.0 ± 1.0	728 ± 29	11.7 ± 1.0	1.7 ± 0.1	18.8 ± 0.2
	10^{-4}	531 ± 30	9.4 ± 1.0	564 ± 32	10 ± 1.1	1.9 ± 0.1	16.0 ± 0.4
H350-20	1	823 ± 38	13.5 ± 0.6	1061 ± 86	17.4 ± 0.8	1.5 ± 0.1	16.8 ± 0.6
	10^{-2}	605 ± 34	11.8 ± 0.4	780 ± 44	15.2 ± 1.7	2.0 ± 0.2	15.8 ± 0.2
	10^{-3}	510 ± 17	10.0 ± 0.3	657 ± 22	12.9 ± 0.5	2.0 ± 0.1	13.6 ± 0.2
	10^{-4}	417 ± 24	7.8 ± 0.2	534 ± 31	10.1 ± 0.3	2.0 ± 0.1	12.2 ± 0.2
H350-40	1	734 ± 76	14.1 ± 1.4	1034 ± 107	19.9 ± 2.0	2.0 ± 0.2	16.8 ± 0.4
	10^{-2}	560 ± 41	13.4 ± 1.2	789 ± 58	18.9 ± 1.7	2.2 ± 0.4	14.9 ± 0.1
	10^{-3}	453 ± 29	9.9 ± 0.5	638 ± 41	13.9 ± 0.7	2.2 ± 0.3	12.7 ± 0.4
	10^{-4}	326 ± 17	7.6 ± 0.4	443 ± 23	10.3 ± 0.5	2.5 ± 0.2	10.7 ± 0.4
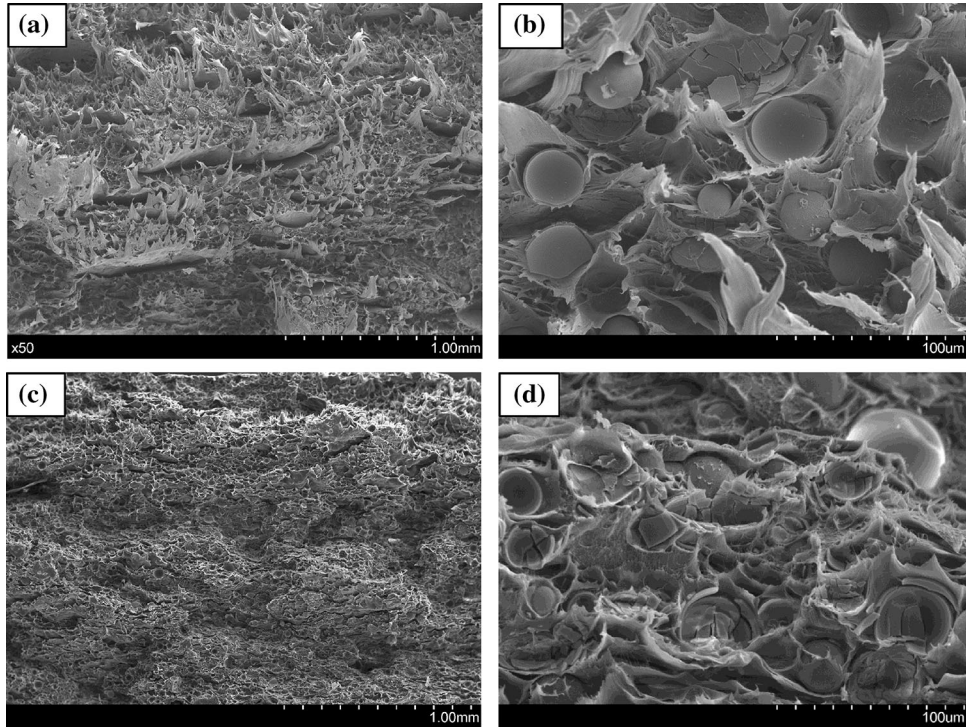
Fig. 4. SEM micrographs (at two different magnifications) of a (a, b) H350-20 specimen and (c, d) H350-40 specimen compression tested at 10^{-3} s^{-1} strain rate.

of matrix porosity in the current 3D-printed specimens. The modulus of H350-40 is the lowest at all strain rates. It is also likely that the irregular or elongated shape of porosity (Fig. 1f) contributes to lowering of the mechanical properties compared with 3D-printed H350-20. Sphericity of voids has been shown to be a factor that affects the mechanical properties of foams.[26] A foam with spherically shaped porosity has a greater modulus than the foam with irregular porosity. The difference in

modulus of 3D-printed and CM materials can be attributed to the chain branching, alignment and cross-linking of HDPE. An increase in the number of processing cycles can increase the degree of chain alignment, branching and cross-linking in the polymer.[27] It has been shown that all these phenomena improve the elastic modulus of a semi-crystalline polymer[28–30] such as HDPE by stiffening the backbones of the polymer chains. It was pointed out that
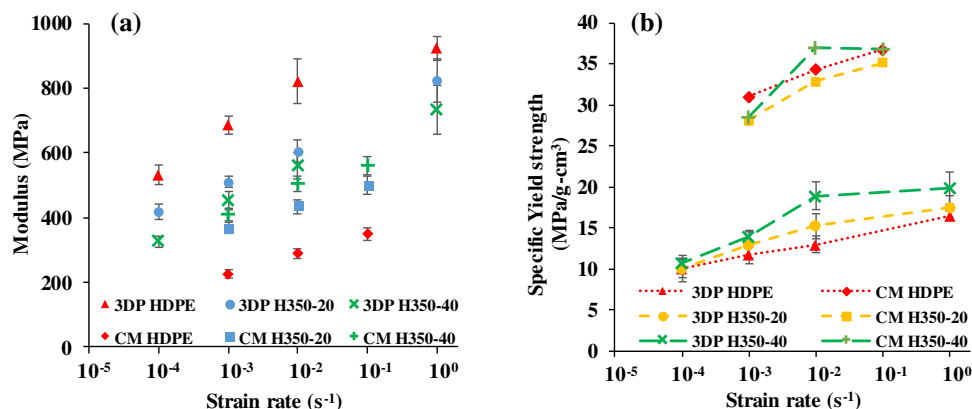
Fig. 5. Comparison of (a) Young's modulus and (b) specific yield strengths at varying strain rates between 3D-printed (current study) and CM materials (data obtained from Ref. 19).

the effect was the opposite for polymers with high levels of crystallinity, i.e., the modulus decreases with greater levels of branching.

The yield strength of the 3D-printed HDPE is higher than that of the syntactic foams (Table I), except at 0.01 s^{-1} strain rate. Similar trends were seen for the CM specimen as well. Compared with the CM specimen, 3D-printed HDPE and its syntactic foams had lower yield strength. This reduction was expected and occurs because of the presence of porosity in the 3D-printed material. It appears that the effect of matrix porosity is stronger on the strength than on the density of the composite. The trend of specific yield strengths of the three materials and comparison with compression-molded specimens are shown in Fig. 5b. The 3D-printed H350-40 shows the highest specific yield strength, followed by H350-20 and HDPE for all strain rates, the difference being more pronounced at higher strain rates.

CONCLUSION

Porous lightweight filaments of three-phase syntactic foams are developed in this work. The filament contains HDPE resin filled with glass microballoons and matrix porosity for potential lightweight applications. These filaments are developed for use in commercial 3D printers. The 3D printing process was also optimized in this work to obtain high-quality prints retaining the porosity in the part. Microscopic examination revealed that the porosity was entrapped in the filaments and retained in the 3D-printed parts, providing low-density syntactic foams. Compression tests were performed on 3D-printed specimens, and the results can be summarized as:

- 3D-printed three-phase syntactic foam parts were up to 11% lighter than the density calculated based on the rule of mixtures.
- An increasing trend in modulus was observed with strain rate for all materials.
- Compared with compression-molded parts con-

taining no matrix porosity, 3D-printed parts had a higher modulus, resulting in improved weight-saving potential due to their lower density.
- Specific yield strength of H350-40 is highest, followed by H350-20 and HDPE, and showed an increasing trend with strain rate.
- Specific yield strength of 3D-printed parts was lower than compression-molded parts because of residual compressive stress build-up during 3D printing.

Syntactic foams are widely used in underwater vehicle structures, where buoyancy and compressive properties are important. It is expected that the availability of porous three-phase syntactic foam filaments will help in developing complex-shaped components for weight-sensitive applications.

ELECTRONIC SUPPLEMENTARY MATERIAL

The online version of this article (https://doi.org/10.1007/s11837-019-03355-5) contains supplementary material, which is available to authorized users.

REFERENCES

1. N. Gupta, D. Pinisetty, and V.C. Shunmugasamy, *Reinforced Polymer Matrix Syntactic Foams* (Cham: Springer, 2013), pp. 1–8.

2. G. Tagliavia, M. Porfiri, and N. Gupta, *Compos. B Eng.* 41, 86 (2010).
3. N. Gupta, S.E. Zeltmann, V.C. Shunmugasamy, and D. Pinisetty, *JOM* 66, 245 (2014).
4. V.C. Shunmugasamy, D. Pinisetty, and N. Gupta, *J. Mater. Sci.* 47, 5596 (2012).
5. V.C. Shunmugasamy, D. Pinisetty, and N. Gupta, *J. Mater. Sci.* 49, 180 (2014).
6. M. Porfiri and N. Gupta, *Compos. B Eng.* 40, 166 (2009).
7. M. Aureli, M. Porfiri, and N. Gupta, *Mech. Mater.* 42, 726 (2010).
8. E. Lawrence and R. Pyrz, *Polym. Polym. Compos.* 9, 227 (2001).
9. B.R. Bharath Kumar, M. Doddamani, S.E. Zeltmann, N. Gupta, M.R. Ramesh, and S. Ramakrishna, *Mater. Des.* 92, 414 (2016).
10. M.L. Jayavardhan, B.R. BharatKumar, M. Doddamani, A.K. Singh, S. Zeltmann, and N. Gupta, *Compos. Part B Eng.* 130, 119 (2017).
11. M. Attaran, *Bus. Horiz.* 60, 677 (2017).
12. F. Ning, W. Cong, J. Qiu, J. Wei, and S. Wang, *Compos. B Eng.* 80, 369 (2015).
13. N. Li, Y. Li, and S. Liu, *J. Mater. Process. Technol.* 238, 218 (2016).
14. G.D. Goh, V. Dikshit, A.P. Nagalingam, G.L. Goh, S. Agarwala, S.L. Sing, J. Wei, and W.Y. Yeong, *Mater. Des.* 137, 79 (2018).
15. A.K. Singh, B. Saltonstall, B. Patil, N. Hoffmann, M. Doddamani, and N. Gupta, *JOM* 70, 310 (2018).
16. A.K. Singh, B. Patil, N. Hoffmann, B. Saltonstall, M. Doddamani, and N. Gupta, *JOM* 70, 303 (2018).
17. G.M. Gladysz, B. Perry, G. Mceachen, and J. Lula, *J. Mater. Sci.* 41, 4085 (2006).
18. M. Narkis, S. Kenig, and M. Puterman, *Polym. Compos.* 5, 159 (1984).
19. M.L. Jayavardhan and M. Doddamani, *Compos. B Eng.* 149, 165 (2018).
20. M.L. Jayavardhan, B.R. Bharath Kumar, M. Doddamani, A.K. Singh, S.E. Zeltmann, and N. Gupta, *Compos. Part B Eng.* 130, 119 (2017).
21. B.R. Bharath Kumar, A.K. Singh, M. Doddamani, D.D. Luong, and N. Gupta, *JOM* 68, 1861 (2016).
22. R. Li, *Mater. Sci. Eng. A* 278, 36 (2000).
23. X. Xu and N. Gupta, *Adv. Theory Simul.* (2019). https://doi.org/10.1002/adts.201800131.
24. X. Xu and N. Gupta, *Materialia* 4, 221 (2018).
25. S.E. Zeltmann, B.R. Bharath Kumar, M. Doddamani, and N. Gupta, *Polymer* 101, 1 (2016).
26. Y. Hangai, H. Kamada, T. Utsunomiya, S. Kitahara, O. Kuwazuru, and N. Yoshikawa, *Materials* 7, 2382 (2014).
27. S. Yin, R. Tuladhar, F. Shi, R. Shanks, M. Combe, and T. Collister, *Polym. Eng. Sci.* 55, 2899 (2015).
28. S. Livshin and M.S. Silverstein, *Macromolecules* 41, 3930 (2008).
29. K. Sehanobish, R.M. Patel, B.A. Croft, S.P. Chum, and C.I. Kao, *J. Appl. Polym. Sci.* 51, 887 (1994).
30. I.M. Ward and J. Sweeney, Structure of polymers.*Mechanical Properties of Solid Polymers*, ed. I.M. Ward and J. Sweeney (New York: Wiley, 2012), p. 1.